Presented at the 29th European PV Solar Energy Conference and Exhibition, 22-26 September 2014, Amsterdam, The Netherlands

MICRO-CRACKS IN SILICON WAFERS AND SOLAR CELLS: DETECTION AND RATING OF MECHANICAL STRENGTH AND ELECTRICAL QUALITY

Matthias Demant[1], Marcus Oswald[2], Tim Welschehold[1], Sebastian Nold[1], Sebastian Bartsch[4], Stephan Schoenfelder[2, 3] and Stefan Rein[1]

[1] Fraunhofer Institute for Solar Energy Systems ISE, 79110 Freiburg, Germany
[2] Fraunhofer Center for Silicon Photovoltaics CSP, 06120 Halle, Germany
[3] Leipzig University of Applied Science, 04277 Leipzig, Germany
[4] Jonas & Redmann Photovoltaics Production Solutions GmbH, 10553 Berlin, Germany

ABSTRACT: In this work, we summarize the basic results of two studies investigating the detection of micro-cracks in as-cut wafers, their impact on fracture strength after texturing (criterion 1) and finally the electrical quality after solar cell production (criterion 2). As a key parameter for quality assessment, the morphology of the artificially induced cracks is reconstructed and quantified in photoluminescence (PL) images of as-cut wafers. As expected, the crack-related sorting parameter showed high correlation to both quality parameters. This enables us to define classification criteria to rate the measured crack morphology in the as-cut stage in terms of the expected fracture strength of the wafer and the expected parallel resistance of the cell, respectively. Based on the presented studies, sorting criteria are evaluated via a receiver operating characteristic (ROC) analysis assuming a specific production load. Moreover, requirements for a PL detection algorithm are derived to achieve the optimal sorting quality according to specific limits for fracture strength and parallel resistance. Cost of Ownership calculations show, that sorting out as-cut wafers prior to cell production can be beneficial if the crack detection system's sorting quality is sufficient.
Keywords: crack, luminescence, detection, fracture strength, shunt, sorting criteria

1 INTRODUCTION

As micro cracks increase mechanical wafer breakage and can affect the shunt behaviour of cells, micro-crack control is essential to increase production yield and can be performed on as-cut mono-crystalline Czochralski (Cz) Si wafers and multi-crystalline (mc) Si wafers. In spite of the control need and the availability of detection techniques, such as the infrared-transmission (IR) or the photoluminescence (PL) technique, micro crack control is often not applied consequently in cell production due to the lack of (i) robust classification criteria and (ii) robust detection algorithms, especially in the case of PL imaging.

For the automatic detection and reconstruction of cracks in PL- but also IR-images various additional defect structures like grain boundaries and saw-marks have to be handled. To this end, a complex machine learning algorithm was extended to crack detection. Our approach is based on a machine-learning algorithm as proposed in [1] on wafer level. We enhance the algorithm by incorporating additional grain boundary information to avoid false positive detections of grain structures as cracks.

On a comprehensive set of artificially damaged wafers we will derive sorting criteria to rate cracks with respect to the expected fracture strength of the wafer based on the measured crack morphology. Since previous studies [1-4] on solar-grade silicon could not reveal the theoretically expected dependency of crack length and fracture strength unambiguously, we try to avoid additional confounding factors. Therefore, the fracture strength of the wafers is determined within a 4-point bending test, which allows a homogeneous stress field in the inner part of the test setup [5] with cracks inserted in the centre region of the wafer. Another influencing factor of inhomogeneous surface is avoided by measuring the wafers after wet chemical texturing.

The impact on cell or module performance of crack structures induced after emitter formation has been analysed in various studies [6-8]. Hereby, a reduction of electrical quality has been ascertained due to cracks with a large spatial extension. Moreover, it has been observed that cracks which are induced in an early process step may lead to shunts [9-11]. Being an additional relevant criterion for the rating of cracks, we investigate the impact of crack morphology measured in the as-cut stage on the electrical quality of the finished solar cell.

In the following sections, we give an overview of our approach to detect cracks and to derive sorting criteria for cracks in terms of fracture strength and electrical quality. A more precise description of approach and experimental details concerning fracture strength is given in [12]. Further information on the rating of the electrical quality is presented in [13]. Additionally, the derived dependencies are analysed with respect to exemplary critical values of fracture strength and parallel resistance, which allows defining the optimal rating criteria of crack morphologies to fulfil the corresponding limits.

2 THEORY AND APPROACH

2.1 Detection of micro-cracks

The detection algorithm is based on a classification of cracks due to a comparison of the crack descriptions with previously trained crack data. An overview of the algorithm is presented in Figure 1. In the first step, the so-called "feature detection", a sparse set of possible crack centres is identified by detecting features, which appear as star or line-like structures. Typically, also recombination-active grain boundaries, which are visible in PL image, may be added to the set of interesting points. To avoid these false detections, the information about grain boundaries is extracted from additional images in the visible range. A key point is excluded from the list of potential crack centres if its position corresponds to the position of a grain boundary. Second, the shape of the remaining cracks are described with a gradient location and orientation histogram (GLOH) - descriptor as introduced in [14]. Hereby, the amplitudes

of the gradients are combined in a histogram which considers the location and gradient orientation. Third, the data were labelled based on the well-known crack positions. A prediction model is trained on the labelled data to classify cracks and non-crack structures using a support vector machine [15]. In case of a positive detection result, the crack is reconstructed by tracing all structures which are following a star-structure beginning from the crack centre. Further details concerning the algorithm are described in [12].

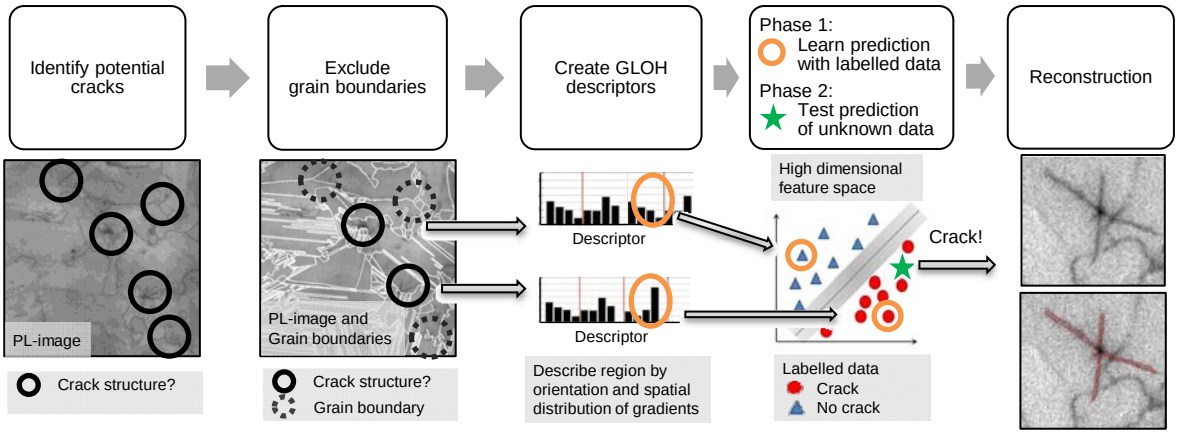

Figure 1: Simple overview of the detection algorithm: After the prediction model is trained on labelled data, a set of "unknown" data, which are not in the training set, can be predicted based on the description of the surrounding region with a GLOH-descriptor.

2.2 Fracture strength

We want to create a link between the morphology of the reconstructed cracks and wafer breakage. Therefore, the fracture strength of the wafers is determined as quality parameter in a 4-point bending setup [5] after the texturing process and compared to the crack length. According to [16, 17], the relation between crack length a and fracture strength σ for line-like cracks in the infinite plate is given by

$$\sigma = K_{Ic} / \left(\sqrt{a/2} \cos^2(\varphi) \right). \qquad (1)$$

The critical fracture toughness K_{Ic} is a material parameter, which depends in crystals on the cleavage planes and thus on grain orientation and varies between 0.89 and 0.92 MPa $m^{-1/2}$ [18]. The influence of crack length onto fracture strength also depends on the orientation φ of the crack perpendicular to load direction. As the crack prefers to propagate along the {110} and {111} plane [19], the crack orientation and shape of the crack segments varies in mc-Si wafers, whereas the cracks show a constant line or x-shaped structure in Cz-Si wafers following the {110} or {111} plane with segments in the direction of $\varphi=\pi/4$ referring the edges of the wafer where the load is applied. We simplify the complex structures of cracks in multi-crystalline wafers by considering the length and orientation of the major-axis a_{major} and minor-axis a_{minor} of the corresponding ellipse with the same normalized second central moments. Therefore, the orientation of the major axis φ_{major} is computed for mc-Si wafers and the orientation of the minor axis is given by $\varphi_{minor}=\varphi_{major}+\pi/2$.

2.3 Electrical quality

Due to the high breakage rates of crack-affected wafers, it is difficult to evaluate sorting criteria based on crack data of as-cut wafers, which indicate the resulting electrical quality of the solar cell. Within our approach of controlled crack introduction, it has been achieved to induce cracks in the dimension of about 1 to 50 mm in mc-Si as well as Cz-Si wafers measured in PL-images, which are on the one hand big enough to be detected by the available system for inline wafer inspection and on the other hand small enough to allow the production of solar cells with low breakage rates. Being a typical indicator for shunts, the parallel resistance R_p is investigated as quality label for a crack sorting criterion which reflects the expected electrical quality. Further cell parameters as the reverse current density can be considered as well as quality label as shown in Ref. [13], but are not presented in this work.

3 EXPERIMENTAL OVERVIEW

3.1 Experimental flow

This section gives a brief overview of the experiments as depicted in Fig. 2. For further details and parameter settings and for issues concerning image acquisition and fracture strength we refer to [12]. For details concerning electrical measurements and solar-cell processing, we refer to [13].

The study has been performed on Cz-Si wafers and mc-Si wafers, which were investigated in sets of different wafer thickness. Primarily, the wafers are marked with an alphanumeric code to be able to identify the samples. The wafers are artificially damaged in the as-cut stage (step 1) by dropping an adjustable punch from a fixed height which allows inducing cracks of macroscopic dimensions in a very controlled manner with the required throughput to generate sufficiently large wafer sets for the test. In

this setup, the wafers were fixed by polyethylene rings in order to avoid air pads between wafer and ground plate, which is necessary to achieve a reproducible damage on both material types. All wafer sets (material type / wafer thickness) are damaged with three different energies. Due to the observed differences in crack length between the two material types, a group with low impact energy was added for Cz-Si wafers and a group of strong impact energy for mc-Si wafers, respectively. The crack position was recorded for the later labelling of the images.

The damaged wafers are inspected in the as-cut stage by means of the PL and IR technique using state-of-the-art wafer inspection systems to create representative control data also available in a manufacturing line. The image processing (step 2) to detect the intentionally induced micro-cracks is accomplished according to the scheme depicted in Figure 1 (see section 2.1). The evaluation and training of the algorithm was based on the labelled data. The morphology of all cracks was determined in PL- images of as-cut wafers with the reconstruction algorithm proposed in [12] based on the well-known crack position. As etching processes are known to be beneficial for the mechanical strength, the Cz-Si and mc-Si samples are subjected to a standard alkaline and acid texturization process, respectively. As a rating label for the measured crack lengths, the fracture strength (step 3) of the wafers has to be determined, which has been performed within a 4-point bending test [5], with the artificial cracks being placed in a homogeneous bending stress field, after wet-chemical texturing of the wafers.

To investigate the impact of cracks onto the electrical quality (step 4), a second set of wafers with varying crack lengths is processed to solar cells using an industrial cell process with aluminium back-surface field in the PV-TEC research line at Fraunhofer ISE [20]. The current-voltage characteristics are determined for all cells.

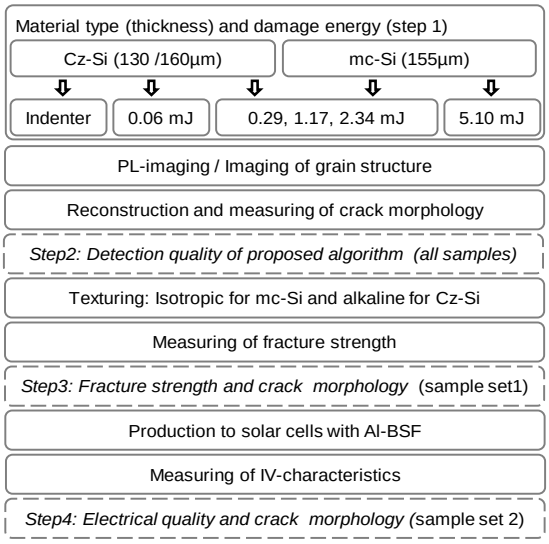

Fig. 2: Overview of the experiment. The dashed lines indicate the evaluation steps.

3.2 Fracture strength from crack morphology

The dependency between crack morphology in the as-cut wafer and fracture strength after wet-chemical etching is investigated based on the reconstruction result of crack structures around the well-known crack positions in the PL-images. Due to complex crack morphologies the major-axis length a_{major} and minor-axis length a_{minor} are selected as basic parameters to describe the crack lengths. The lengths of the cracks are corrected by subtracting 0.5 mm at each side of the crack to prevent an overestimation of crack lengths due to charge carrier diffusion and image blurring. The data were evaluated according to eq.1 assuming a fixed critical fracture toughness for both materials with K_{Ic}=0.92 MPa $m^{-1/2}$. The expected fracture strengths σ_{major} and σ_{minor} are calculated for both axis of the crack considering the orientations φ_{major} and φ_{minor} respectively. Depending on the orientation of the crack, the minor-axis length may lead to more critical fracture strength. In this case, the crack axis with the most critical fracture strength $\sigma_{Pred}=\min(\sigma_{major}, \sigma_{minor})$ was selected as dominating structure.

4 EXPERIMENTAL RESULTS

4.1 Fracture strength and crack morphology

The plots in Fig. 3 show the measured fracture strength as a function of predicted fracture strength from crack length of PL-images for Cz-Si wafers (a) and mc-Si wafers (b). The colour indicates the projected crack lengths $a_{Projected}$ of the crack segment onto the line orthogonal to the load direction with $a_{Projected}=\min(a_{major}\cos(\varphi_{major}), a_{minor}\cos(\varphi_{minor}))$, which turns out to be a relevant quantity as discussed in detail in [12].

The results show a strong correlation for Cz-Si wafers. The measured fracture strength varies corresponding to the predicted fracture strength. Prediction quality decreases for very small cracks and high fracture strengths, respectively. This is expected from functional dependency between crack length and fracture strength in equation 1 which exhibits a steep slope for small crack lengths. Although the correlation is lower for mc-Si wafers, samples with reduced fracture strength can be identified based on to the predicted fracture strengths.

4.2 Sorting crack morphology by fracture strength

The correlation between fracture strength and crack length can be used to define sorting criteria for a given manufacturing equipment or production line, as well as to define demands onto the crack detection algorithm. First, sorting criteria can be evolved for different machine capabilities to handle wafers down to critical fracture strength $\sigma_{critical}$. We assume that wafers with a fracture strength lower $\sigma_{critical}$ break during solar cell production. As a scatter can be observed in the measured fracture strength σ and the predicted fracture strength σ_{Pred} a more accurate threshold can be determined by optimizing the relation between the ability to detect critical samples by considering the sensitivity (true positive rate TPR) of the classification on the one hand and the ability to avoid falsely as critical classified samples by considering parameters of the false positive rate or the precision on

the other hand. The values are defined as

$$\begin{aligned} \text{TPR} &= \text{Sensitivity} = \#(D \cap C)/\#C \\ \text{FPR} &= 1 - \text{Specificity} = \#(D \cap \overline{C})/\#\overline{C} \\ \text{Precision} &= \#(D \cap C)/\#D \end{aligned} \qquad (2)$$

with the cardinality # of the set of detected samples D, which are classified as critical, the set of truly critical samples C and the set of non-critical samples $\overline{C}$.

The combinations of sensitivity and specificity are illustrated by the receiver operating characteristic (ROC curve) [21] in Fig. 3 (c). Each line indicates the resulting quality of the classifier with varying threshold for a specific material class and critical fracture strength $\sigma_{critical}$. The diagonal black line indicates the ROC curve of a random guess with a ROC area of 0.5. The area beneath the curve is an indicator for the quality of the binary classifier. Optimally, these values are very small (ROC area=0) or near the maximum value (ROC area=1). Exemplary values for critical fracture strength were selected according to the distribution of fracture strength of given data. Due to the increased range of fracture strength in the Cz-Si material group, critical fracture strengths of $\sigma_{critical1,Cz}$=75 MPa and $\sigma_{critical2,Cz}$=100 MPa were selected for the ROC analysis. Since all mc-Si data show a reduced fracture strength, the ROC analysis is performed for critical fracture strengths $\sigma_{critical1,mc}$=50 MPa and $\sigma_{critical2,mc}$=65 MPa. According to the critical value the data are split into samples, which will withstand the mechanical stress and samples which will break during solar cell production. Based on the crack related parameter σ_{Pred} the wafers can be classified to predict the breakage of the wafer. The decision value for σ_{Pred} is varied and the related sorting parameters sensitivity and specificity are computed to determine the best threshold. The characteristics of the ROC curves are listed in Table I. For Cz-Si wafers, the area of the ROC curve is nearly 1 for a threshold value for critical fracture strength $\sigma_{critical1,Cz}$ and decreases with increasing critical fracture strength. The threshold value with the highest product of sensitivity and specificity $\sigma_{Pred,opt}$ and the corresponding crack length $a_{Pred,opt}$ are also indicated assuming a crack orientation of $\varphi_{Pred,opt}=\pi/4$. The results in the table can be interpreted as following: A crack in a Cz-Si wafer with length $a > 3.4$mm and orientation of $\varphi = \pi/4$ should be sorted out, since the ROC analysis indicates that the wafer will break with high confidence when a load of 75MPa is applied. For smaller cracks the quality of the rating reduces as the false negative rate increases.

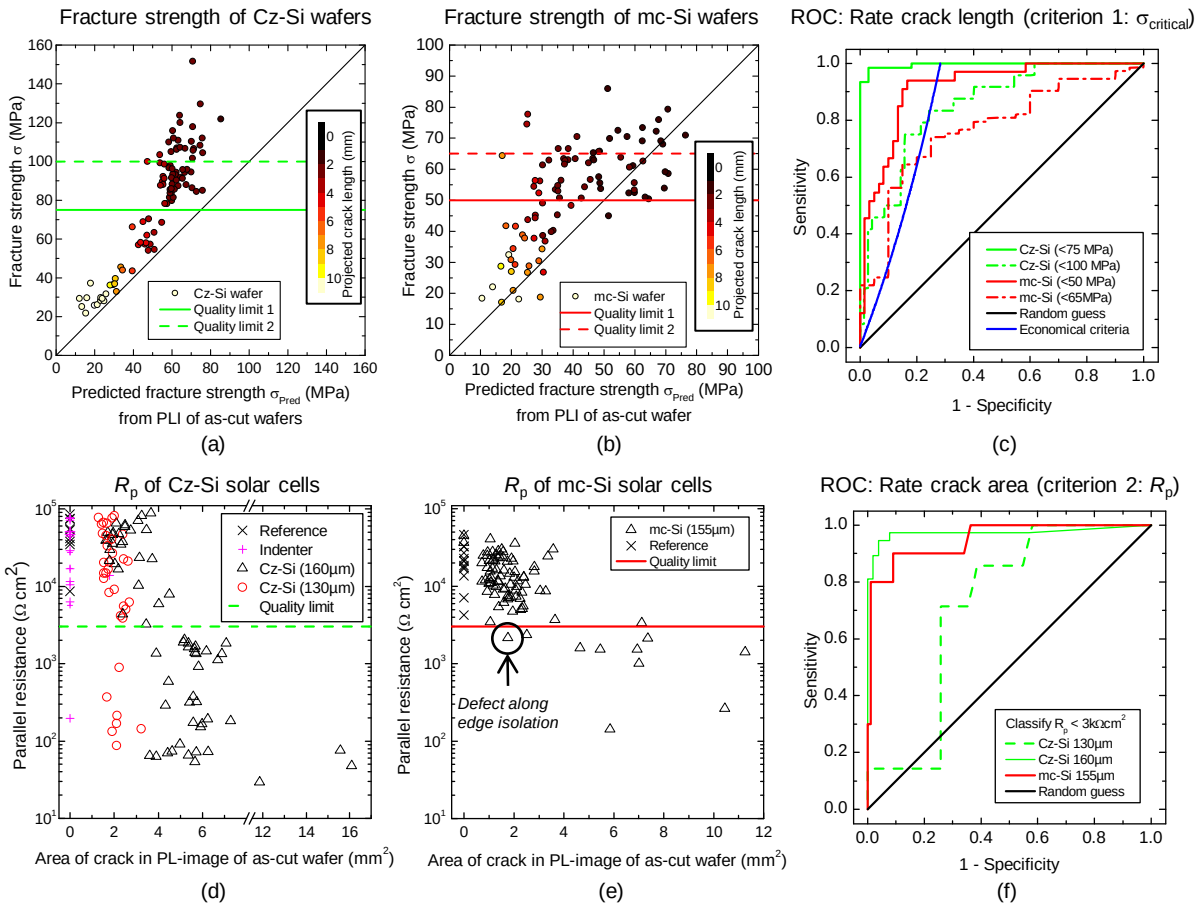

Fig. 3: Comparison of crack-related quality data measured on as-cut wafers to fracture strength (upper row) and parallel resistance (lower row) of Cz-Si (left column) and mc-Si (middle column) wafers and solar cells. The right column displays the combined ROC curves of both material types according to the quality data in each row. Each ROC curve analyses the classification quality considering a specific quality limit by varying the crack related parameter measured in the as-cut stage as discrimination threshold. The blue line in the ROC curves represents an exemplary quality limit for crack detection systems for Cz-Si material based on a cost of ownership analysis [22]. If the crack detection system achieves quality parameters placed on the left side of the line the system works profitable.

Table I: Receiver operating characteristics: The column 'criteria' indicates the range of critical σ or R_p-values which should be sorted out. The ROC-area is the area under the ROC curve which reflects the quality of the sorting parameter in general. For investigations on fracture mechanics $\sigma_{Pred,opt}$ is the threshold for the predicted fracture strength σ_{Pred} with the maximum product of sensitivity and specificity and $a_{Pred,opt}$ the corresponding crack length for cracks with orientation of $\varphi = \pi/4$. The area A of the crack was selected as most important parameter to rate the crack morphology with respect to R_p values and the optimum sorting criteria A_{opt} was computed.

	Criteria	ROC-area	$\sigma_{Pred,opt}$	$a_{Pred,opt}$
Cz-Si	$\sigma < 75$MPa	0.99	53.4MPa	3.4mm
	$\sigma < 100$MPa	0.85	63.7MPa	2.7mm
mc-Si	$\sigma < 50$MPa	0.92	35.7MPa	6.3mm
	$\sigma < 65$MPa	0.77	47.5MPa	4.0mm

	Criteria	ROC-area	A_{opt}
Cz-Si 130µm	$R_p < 3k\Omega cm^2$	0.71	2.1mm^2
Cz-Si 160µm	$R_p < 3k\Omega cm^2$	0.97	3.8mm^2
mc-Si 155µm	$R_p < 3k\Omega cm^2$	0.95	2.5mm^2 or 4mm^2

4.1 Electrical quality and crack morphology

A major set of pre-damaged wafers could be processed to solar cells despite the artificially induced cracks. Efficiencies of the damaged solar cells ranged between 18.2% and 9.6% for the Cz-Si wafers and 16.2% and 14.0% for the mc-Si wafers. As expected, the analysis of current-voltage characteristics revealed that losses in wafer efficiency follow the reduced values of the parallel resistance according to the two-diode model, as shown in [13]. To analyse the impact of the crack onto the parallel resistance the area A of reduced luminescence intensity surrounding the crack centre was quantified as crack-related sorting parameter in the as-cut stage. The correlation of crack area and parallel resistance is depicted in Fig. 3(d) and (e) for Cz-Si and mc-Si material, respectively. Large micro-cracks tend to lead to stronger shunts. Nevertheless, for Cz-Si material also small cracks strongly affect the electrical quality of the cell. An explanation is given in the thickness-dependent analysis. Micro-cracks in Cz-Si wafers with thickness of 130µm lead to reduced R_p-values. Unfortunately, thin Cz-Si wafers broke during solar cell production due to the large micro-cracks. For mc-Si cells, the R_p-related decrease in cell efficiency is weaker.

4.2 Sorting crack morphologies by parallel resistance

To classify the electrical quality of the damaged wafers, a parallel resistance below 3 kΩcm^2 can be identified as very critical value. Following the two-diode model for the given data set a reduction of the parallel resistance from 100 kΩcm^2 to 3 kΩcm^2 will lead to losses in efficiency of about 0.5%$_{rel}$. The ROC-curves in Fig. 3 depict good classification results for mc-Si wafers as well as for Cz-Si wafers with thickness of 160µm. Cracks with area A greater than approximately 3.8 mm^2 should be sorted out to avoid strong shunts. The group of thinner Cz-Si wafers could not be classified accurately, as even small cracks can result in severe shunts and low parallel resistance.

4.3 Detection results

Micro-cracks in PL-images were analyzed according to the algorithm depicted in Figure 1. As an enhancement to the algorithm published in [1], spatially resolved information about the grain boundaries was added to the classification scheme. The additional data have been gained from surface inspection in the visible range in reflexion mode. The approach was evaluated with a set of multi-crystalline wafers. The algorithm was analysed applying a 10-fold cross validation. Hereby, the wafer data was split into 10 groups. Each group of wafers is evaluated by training the classifier based on the remaining 9 groups. Despite disturbing dislocations and grain boundaries, cracks could be detected with a precision of 91.1% and sensitivity of 80.4% for small cracks with crack length a>3mm. By this means, we achieved an increase in precision of 18.6% compared to 72.5% and an increase in sensitivity of 15.4% from 65% which could be achieved evaluating the same set of small cracks without additional grain boundary information. The optimum relation of sensitivity and precision can be adjusted by means of parameter settings with respect to economic considerations. In this case, the prediction was optimized by maximizing the F-measure, which is the harmonic mean of precision and sensitivity. The presented approach can also be extended to detect cracks in electroluminescence images of solar cells.

5 DISCUSSION

5.1 Quality rating of fracture strength

The length of the micro-cracks and the fracture strength follow the functional dependency expected from theoretical crack mechanics, which is shown in detail in Ref. [12] and, to our knowledge, has not yet been proven experimentally in solar grade silicon, especially not for such a broad range of crack lengths.

The ROC curves in Fig. 3 (c) illustrate the high performance of the classifier for critical fracture strength of 75 MPa. However, this classifier performance decreases as the critical fracture strength increases which corresponds to a decreasing critical crack length.

For Cz-Si wafers with comparatively small crack lengths $a < 2$mm a large scatter can be observed, which can be related to the limited spatial resolution of the PL-imaging system or inhomogeneous crack structures. The classification schemes can be improved by increasing the sharpness of the PL-images using a stronger but shorter duration of excitation. Imaging techniques with higher resolution can be evaluated, but may also fail to reconstruct the cracks precisely, as shown for an infrared transmission setup in Ref. [1]. The sorting criterion with the largest product of sensitivity and specificity is a good setting for a specific loading scheme. The corresponding critical crack length $a_{Pred,opt}$ (see Table I) indicates that samples with smaller crack lengths should pass the breakage criteria and should not be sorted out. Therefore, the PL-detection should at least identify cracks with a length of $a_{Pred,opt}$ to achieve optimal rating values for the applied loading scheme.

The results of fracture strength for mc-Si wafer show a larger scatter, as shown in Fig. 3 (b). This makes the definition of a sorting criterion for mc-Si wafers more complex. The ROC area is decreased for mc-Si wafers

compared to the results for Cz-Si wafers. The increased scatter can partly be explained by the variation of critical fracture toughness due to grain orientation and crack propagation [18]. Second, the morphology of the cracks shows different characteristics in mc-Si wafers, as the shape and the orientation of the cracks differ. Third, the reconstruction may fail due to cracks near dislocations. Furthermore, the dislocation density influences the fracture strength [23]. In spite of these challenges, a classification for critical fracture strength of 50 MPa is applicable. For higher loadings within the solar cell process, classification becomes difficult as shown in Fig. 3 (b).

5.2 Quality rating of parallel resistance

Considering the electrical quality of the wafers, the Cz-Si samples showed higher shunt values than the mc-Si wafers. The classification of wafers based on the crack area (the region of reduced luminescence intensity) to rate the parallel resistance R_P<3kΩcm^{2}of the solar cells could be accomplished for wafers with thickness greater 150µm. For the Cz-Si wafers with thickness of 130µm, even samples with very small cracks showed a reduced parallel resistance. As shown in [13], the shunt strength at a crack can be related to the width of the crack channel, as aluminum paste can be squeezed through enhanced crack channels and is discussed in more detail.

5.3 Economic considerations

The requirements of a crack detection system can be rated economically by applying a cost of ownership analysis. Hereby, different parameters like the input wafer cost, cell production cost and breakage induced yield loss have to be considered. A model to evaluate the requirements of a crack detection system was published in [22]. For specific circumstances, the specification of a system can be derived as a function of sensitivity and specificity of the detection quality. The blue line in Fig. 3 (c) represents an exemplary requirement specification based on the cost of ownership analysis in [22]. It can be interpreted as quality limit of the detection algorithm. Under the assumption that the cracks of the specific size can be detected, the specificity and sensitivity of the rating scheme should be located above the requirement specification. In our example, the rating scheme developed in this work is beneficial to rate critical fracture strength of 75 MPa for Cz-Si wafers (solid green line) and 50 MPa for mc-Si wafers (solid read line). If the critical fracture strength is further increased to 100 MPa for Cz-Si wafers (dash-dotted green line) and 65 MPa for mc-Si wafers (dash-dotted red line) the range of economic beneficial thresholds is more restricted. Thus, the choice of the sorting criteria has to be met more carefully.

6 CONCLUSION

We briefly summarized the experimental results of two studies related to the sorting of wafers based on crack data measured in PL-images of as-cut wafers. The analysis of the elaborated correlations via ROC curves illustrated the capabilities to derive sorting criteria based on morphological crack information in early process steps regarding the fracture strength of textured wafers and the parallel resistance of the processed solar-cells. Hereby mc-Si as well as Cz-Si wafers and solar cells with intentionally induced micro-cracks in as-cut stage have been investigated.

Our results on fracture strength σ and crack length a follow the theoretical relation for a crack length range between 1 and 50 mm in textured wafers, and allow us to derive sorting criteria, which depend on the maximum stress in the production line. A maximum crack length around 3.4 mm must not be exceeded to ensure minimum fracture strength of 75 MPa for Cz-Si wafers. Good classification criteria with a threshold of 6.3 mm can be achieved for mc-Si wafers for fracture strength of 50 MPa. A more relevant threshold can be determined considering the cost of ownership of the crack detection system for different settings within the ROC analysis. Furthermore, the classification scheme of micro-cracks according to fracture strength can be transferred to other crack detection systems.

Also the electrical cell quality can be predicted from the crack morphology via a material-dependent rating scheme: Cz-Si wafers and mc-Si wafers with thickness of 160 µm show shunts for crack area greater than about 4 mm^2. For thin Cz-Si wafers with thickness of 130µm small cracks can lead to shunts.

We introduce an enhanced machine learning scheme to detect cracks in PL- images of mc-Si wafers. The detection algorithm yields good performance in PL-images with a precision of 91.1% and sensitivity of 80.4% for crack length greater than 3 mm. The additional grain information reduces the amount of false positive detections in mc-Si wafers significantly. The machine learning approach is also applicable for IR-Transmission systems.

7 ACKOWLEDGEMENTS

This work has been supported by the German federal ministry of education and research (BMBF) within the framework of the project "xµ-Zellen Phase 2" (03SF0399B and 03SF0399D).

8 LITERATURE

1. Demant, M., et al. *Detection and analysis of micro-cracks in multi-crystalline silicon wafers during solar cell production*. in *37th IEEE Photovoltaic Specialists Conference, PVSC*. 2011. Seattle, WA, USA.
2. Gustafsson, J., et al. *Mechanical stress tests on mc-si wafers with microcracks*. in *23rd European Photovoltaic Solar Energy Conference*. 2008. Valencia, Spain.
3. Trautmann, M., et al. *Inline microcrack detection and mechanical stability of silicon wafers*. in *Proceedings of the 25th European Photovoltaic Solar Energy Conference and Exhibition*. 2010. Valencia, Spain.
4. Trautmann, M., et al. *Non-contact microcrack detection from as-cut wafer to finished solar*. in *Photovoltaic Specialists Conference (PVSC), 2012 38th IEEE*. 2012.
5. Schoenfelder, S., A. Bohne, and J. Bagdahn. *Comparison of test methods for strength characterization of thin solar wafers*. in *Proceedings of the 22nd European Photovoltaic Solar Energy Conference*. 2007. Milan, Italy.
6. Huster, F., et al. *Shunts in silicon solar cells below screen printed silver contacts*. in *Proceedings of the 19th European Photovoltaic Solar Energy*

Conference. 2004. Paris, France: WIP-Munich, ETA-Florence.
7. Köntges, M., et al., *The risk of power loss in crystalline silicon based photovoltaic modules due to micro-cracks.* Solar Energy Materials and Solar Cells, 2011. **95**(4): p. 1131-1137.
8. Pletzer, T.M., et al., *Influence of cracks on the local current–voltage parameters of silicon solar cells.* Progress in Photovoltaics: Research and Applications, 2013.
9. Breitenstein, O., et al., *Shunt types in crystalline silicon solar cells.* Progress in Photovoltaics: Research and Applications, 2004. **12**(7): p. 529-538.
10. Breitenstein, O., et al., *Quantitative evaluation of electroluminescence images of solar cells.* Physica Status Solidi RRL, 2010. **4**(1): p. 7-9.
11. Breitenstein, O., et al., *Influence of defects on solar cell characteristics.* Solid State Phenomena, 2010. **156**: p. 1-10.
12. Demant, M., et al., *Micro-cracks in silicon wafers I: Inline detection and implications of crack morphology on wafer strength.* to be submitted to IEEE, Journal of Photovoltaics.
13. Demant, M., et al., *Micro-cracks in silicon wafers II: Implications on solar cell characteristics, statistics and physical origin.* to be submitted to IEEE, Journal of Photovoltaics.
14. Mikolajczyk, K. and C. Schmid, *A performance evaluation of local descriptors.* IEEE Transactions on Pattern Analysis & Machine Intelligence, 2005. **27**(10): p. 1615-1630.
15. Chang, C.-C. and C.-J. Lin, *Libsvm: A library for support vector machines.* ACM Transactions on Intelligent Systems and Technology (TIST), 2011. **2**(3): p. 27.
16. Murakami, Y., *Stress intensity factors handbook*. 1987, Elsevier Science Limited. p. 914-915.
17. Sih, G.C., P.C. Paris, and F. Erdogan, *Crack-tip, stress-intensity factors for plane extension and plate bending problems.* Journal of applied mechanics, 1962. **29**(2): p. 306-312.
18. Pérez, R. and P. Gumbsch, *Directional anisotropy in the cleavage fracture of silicon.* Physical Review Letters, 2000. **84**(23): p. 5347-5350.
19. Michot, G., *Fundamentals of silicon fracture.* Crystal Properties & Preparation, 1988. **17–18**: p. 55-98.
20. Biro, D., et al. *Pv-tec: Retrospection to the three years of operation of a production oriented research platform*. in *Proceedings of the 24th European Photovoltaic Solar Energy Conference*. 2009. Hamburg, Germany.
21. Witten, I.H. and E. Frank, *Data mining : Practical machine learning tools and techniques with java implementations*. 1999, San Francisco, Calif.: Morgan Kaufmann.
22. Aßmus, M., et al., *Performance requirements of crack detection systems in silicon solar cell production.* Energy Procedia, 2012. **27**: p. 147-153.
23. Oswald, M., S. Schoenfelder, and R.D. Donno. *Modeling of multicrystalline silicon wafers considering microstructural properties*. in *5th International Workshop on Crystalline Silicon Solar Cells*. 2011. Boston, USA.